Catalysis Today 143 (2009) 211–217

Contents lists available at ScienceDirect

Catalysis Today

journal homepage: www.elsevier.com/locate/cattod

Redox-catalytic correlations in oxidised copper-ceria CO-PROX catalysts

A. Martínez-Arias [a,*], D. Gamarra [a], M. Fernández-García [a], A. Hornés [a], P. Bera [a], Zs. Koppány [b], Z. Schay [b]

[a] Instituto de Catálisis y Petroleoquímica, CSIC, C/Marie Curie 2, Campus Cantoblanco, 28049 Madrid, Spain
[b] Institute of Isotopes, Hungarian Academy of Sciences, H 1525-Budapest, Hungary

ARTICLE INFO

Article history:
Available online 5 November 2008

Keywords:
CuO-CeO_2 catalysts
CO-PROX
Operando-DRIFTS
Operando-XANES
H_2-TPR
CO-TPR

ABSTRACT

Four nanostructured oxidised copper-cerium catalysts prepared by two different methods (impregnation of ceria and coprecipitation of the two components within reverse microemulsions) with varying copper loadings have been examined with the aim of establishing correlations between redox and catalytic properties for preferential oxidation of CO in H_2-rich streams. The analysis is based on ex situ TPR examination both with H_2 or CO as well as *operando* spectroscopic exploration by DRIFTS and XANES, additionally complemented by conventional catalytic tests. The results reveal redox promoting effects on copper oxide reduction and allow establishing a model of the catalytic behaviour of this type of catalysts which can provide keys to control their CO-PROX catalytic properties.

1. Introduction

Production of H_2 for polymer fuel cells (PEMFC) is usually accomplished by a multi-step process that includes catalytic reforming of hydrocarbons or oxygenated hydrocarbons followed by water gas-shift (WGS) [1,2]. The gas stream obtained after these processes presents in most cases a relatively high CO concentration that disallows efficient handling of the fuel by the Pt alloy anode usually employed in the PEMFC. Preferential (or selective) oxidation of CO in the H_2-rich stream resulting from such processes (CO-PROX) has been recognized as one of the most straightforward and cost-effective methods to achieve acceptable CO concentrations (below ca. 100 ppm) [3–7].

Catalysts based on closely interacting copper oxide and ceria have shown promising properties in terms of activity and selectivity, while their lower cost with respect to formulations based on noble metals could make them strongly competitive [3,4,6–15]. The particular ability of this class of catalysts for the CO-PROX or related processes has been essentially attributed to the synergistic redox properties produced upon formation of copper oxide-ceria interfacial sites [4,6,9,10,16–21]. In this sense, generally speaking, the properties of copper oxide entities for CO oxidation promotion apparently depend strongly on their dispersion degree and/or related degree of interaction with ceria [10,16,17,22]. Additionally, incorporation of copper into the fluorite network of ceria can induce important modifications on its chemical properties [23–26]. Nevertheless, details are lacking with respect to the nature of the species or processes involved in the reaction mechanism and/or their respective evolutions during the catalytic process as well as the role of redox promoting effects on the catalytic properties [6,9,16].

Within this context, the present work mainly revises recent contributions from our laboratory which provide insights into these issues and the results are complemented by classical TPR exploration of the systems [27–29], considering also the generalized use of the latter for analysis of their redox properties [30–33]. Thus, four catalysts differing in the preparation method employed have been examined by H_2-TPR and CO-TPR techniques as well as by *operando*-DRIFTS and XANES, in order to provide a complete explanation of CO-PROX catalytic properties of this type of catalysts; complete structural, morphological and chemical characterization of the four catalysts can be found elsewhere [27,28]. The results allow establishing a model of their catalytic properties and can serve as a useful tool to achieve a controlled design of this type of catalysts.

2. Experimental

Two Cu-doped ceria samples, labelled as $Ce_{1-x}Cu_xO_2$ ($x = 0.05$ and 0.2) were prepared with a modified reverse microemulsion method [25,34]. Briefly, the precursors (copper (II) and cerium (III) nitrates from Aldrich) were introduced in a reverse microemulsion

* Corresponding author.
E-mail address: amartinez@icp.csic.es (A. Martínez-Arias).

0920-5861/$ – see front matter © 2008 Elsevier B.V. All rights reserved.
doi:10.1016/j.cattod.2008.09.018

(water in oil) using *n*-heptane as the organic phase, Triton X-100 (Aldrich) as surfactant, and hexanol as cosurfactant. Then, this suspension was mixed with another similar suspension containing an alkali solution (TMAH, Aldrich) in its aqueous phase in order to coprecipitate the cations. The resulting mixtures were stirred for 24 h, centrifuged, decanted, and rinsed with methanol. Finally, the solid portion was dried overnight at 373 K, and the resulting powders were calcined under air at 773 K for 2 h. ICP-AES chemical analysis of these samples confirmed quantitative precipitation of both Cu and Ce cations. Two samples of copper oxide supported on CeO_2 (Cu wt.% of 1.0 and 5.0, denoted as $1CuO/CeO_2$ and $5CuO/CeO_2$, respectively; these correspond to Cu/Ce at. ratios of 0.022 and 0.116, respectively) were prepared by incipient wetness impregnation of a CeO_2 support prepared by microemulsion (in a similar manner as described above) with copper nitrate aqueous solutions. Following impregnation, the samples were dried overnight at 373 K and finally were calcined under air at 773 K for 2 h.

The catalysts calcined in situ (under oxygen diluted in Ar at 773 K) were tested in a glass tubular catalytic reactor for their activity under an atmospheric pressure flow (using mass flow controllers to prepare the reactant mixture) of 1% CO, 1.25% O_2 and 50% H_2 (Ar balance), at a rate of 1×10^3 cm^3 min^{-1} g^{-1} (roughly corresponding to 80,000 h^{-1} GHSV) and using a heating ramp of 5 K min^{-1} up to 523 K. Analysis of the feed and outlet gas streams was done by gas infrared (PerkinElmer FTIR spectrometer model 1725X, coupled to a multiple reflection transmission cell – Infrared Analysis Inc. "long path gas minicell", 2.4 m path length, *ca.* 130 cm^3 internal volume) while a paramagnetic analyser (Servomex 540 A) was used to analyse the O_2 concentration. No products other than those resulting from CO or H_2 combustion (i.e. CO_2 and H_2O; only a residual contribution of possible WGS or reverse WGS reactions, taking place in any case at temperatures higher than ca. 453 K, was estimated from mass balance under the conditions employed; this was also confirmed by independent tests including CO_2 or H_2O as reactants) were detected in the course of the runs, in agreement with previous results on catalysts of this type [6,9,11,22]. On this basis, values of percentage conversion and selectivity in the CO-PROX process are defined as:

$$X_{O_2} = \frac{F_{O_2}^{in} - F_{O_2}^{out}}{F_{O_2}^{in}} \times 100, \quad X_{CO} = \frac{F_{CO}^{in} - F_{CO}^{out}}{F_{CO}^{in}} \times 100,$$

$$S_{CO_2} = \frac{X_{CO}}{2.5X_{O_2}} \times 100$$

where X and S are percentage conversion and selectivity, respectively, and F is the (inlet or outlet) molar flow of the indicated gas.

Temperature programmed reduction under hydrogen (H_2-TPR) was measured in a flow system using $1\%H_2$/Ar premixed gases with flow rate of 30 cm^3 min^{-1}. A cold trap filled with liquid nitrogen was placed after the reactor to remove water. The system was equipped with a thermal conductivity detector. About 40 mg catalyst was placed into a quartz U-tube and calcined in $5\%O_2$/He at 773 K for 1 h using 40 cm^3 min^{-1} flow rate and 10 K min^{-1} ramp. The sample was cooled to room temperature, purged with Ar and after switching to the reducing gas mixture it was heated to 773 K using 10 K min^{-1} ramp. Temperature programmed reduction experiments employing CO as a reductant (CO-TPR) were performed with a Pfeiffer Omnistar mass spectrometer (MS) monitoring the m/z ratios of 2 (He), 12 (C), 16 (O), 28 (CO) and 44 (CO_2). Prior to the run, ca. 150 mg of sample was calcined in situ at 773 K under flow of 15% O_2/He for 2 h and then the sample was cooled to room temperature in the gas flow, purged under inert gas and exposed to 5% CO/He at that temperature for 15 min. Finally, the sample temperature was raised under 5% CO/He using a ramp of 10 K min^{-1} and a flow of 50 cm^3 min^{-1}.

Operando-DRIFTS analysis was carried out using a Bruker Equinox 55 FTIR spectrometer fitted with an MCT detector. The DRIFTS cell (Harrick) was fitted with CaF_2 windows and a heating cartridge that allowed samples to be heated to 773 K. Aliquots of *ca.* 100 mg were calcined in situ (in a similar way as employed for the catalytic tests, vide supra) and then cooled to 298 K under diluted oxygen before introducing the reaction mixture and heating in a stepped way, recording one spectrum (average of 50 scans at 4 cm^{-1} resolution) typically every 10 K after the signal of different monitored gases (analysed on line by means of a quadrupole mass spectrometer Pfeiffer Omnistar) becomes constant (i.e. steady conditions). The gas mixture (1% CO + 1.25% O_2 + 50% H_2 in He) was prepared using mass flow controllers with *ca.* 100 cm^3 min^{-1} passing through the catalyst bed at atmospheric pressure, which corresponds to conditions similar to those employed for the reaction tests with the tubular reactor.

X-ray absorption near edge structure (XANES) experiments at the Cu-K- and Ce L_{III}-edges were performed at station 7.1 of the SRS (Daresbury, UK) synchrotron. A Si(1 1 1) double-crystal monochromator was used in conjunction with a rejection mirror to minimise the harmonic content of the beam. Transmission experiments were carried out using noble gas- or N_2/O_2-filled ionisation chambers as detector. The energy scale was simultaneously calibrated by measuring a Cu foil or a pure CeO_2 disc using a third ionisation chamber. Self-supporting discs were employed (absorbance 0.5–1.0) and placed in a controlled-atmosphere home made cell for in situ treatment. Analysis of gases was performed on line by means of a Pfeiffer Omnistar quadrupole mass spectrometer. All samples were pretreated under diluted oxygen at 773 K and XANES spectra were taken in the presence of a CO + O_2 + H_2 flowing mixture (similar to the one employed for the DRIFTS experiments) during a 2 K min^{-1} temperature ramp up to 573 K. The series of spectra were analyzed by using principal factor analysis (PCA), details of which can be found elsewhere [35].

3. Results and discussion

Main characteristics of the catalysts at structural, morphological and electronic levels, on the basis of XRD, Raman, HRTEM-XEDS, S_{BET} measurements and XPS were reported in a former contribution [27]. A summary of those results is given hereafter and some relevant data are collected in Table 1. XRD displayed only

Table 1
Main textural and structural characteristics of the copper-ceria catalysts examined in this work [27].

Sample	S_{BET}[a] (m^2 g^{-1})	Lattice parameter[b] (Å)	Crystal size (nm)	Phases detected[c]
$1CuO/CeO_2$	107	5.410	7.8	Fluorite CeO_2
$5CuO/CeO_2$	101	5.413	8.1	Fluorite CeO_2, tenorite CuO
$Ce_{0.95}Cu_{0.05}O_2$	130	5.410	7.0	Fluorite $Ce_{1-x}Cu_xO_2$
$Ce_{0.8}Cu_{0.2}O_2$	151	5.413	6.6	Fluorite $Ce_{1-x}Cu_xO_2$

[a] S_{BET} for the bare CeO_2 support was of 130 m^2 g^{-1} [27].
[b] For the fluorite phase.
[c] Based on XRD and Raman [27].

peaks corresponding to the fluorite structure of ceria, except for the $5CuO/CeO_2$ for which weak and narrow peaks of tenorite CuO were detected. As shown in Table 1, lattice parameters estimated from XRD analysis of the fluorite peaks are close to that expected for pure ceria for all the samples. It must be however considered that copper introduction into the ceria fluorite lattice is not expected to induce significant changes in this parameter [19,20,24,25,27]. Indeed, analysis of lattice microstrain (derived from XRD results) and Raman results revealed significant differences between samples prepared by impregnation and microemulsion-coprecipitation. These have been related to the fact that, as expected, copper remains essentially at the sample surface in the former samples while copper (at least a part of it) appears to be incorporated into the ceria fluorite lattice in the latter [25,27]. Nevertheless, a certain copper surface segregation, increasing with the copper loading, appears evident in the systems prepared by microemulsion-coprecipitation, as evidenced mainly by XEDS and Ar^+-sputtering XPS analyses [27]. Therefore, the catalysts of the $Ce_{1-x}Cu_xO_2$ series can be probably better described as $CuO/Ce_{1-z}Cu_zO_2$ (with the amount of segregated CuO increasing with x), since single solid solution of the copper is not fully achieved. In turn, although CuO-type clusters dispersed on the ceria support apparently predominate for the two $x CuO/CeO_2$ catalysts, differences between them have been shown to be related, as mentioned above, to the presence of large crystalline CuO particles, in accordance also with electron microscopy investigation [27], in $5CuO/CeO_2$. This is related to having exceeded the copper oxide dispersion capacity of the CeO_2 support, as already observed for a sample with 3 wt.% Cu [27]. On the other hand, copper incorporation induces some surface area decrease in the samples prepared by impregnation, probably due to some copper covering of interparticle pores (Table 1). In contrast, the surface area increases with the copper amount for the samples prepared by microemulsion-coprecipitation, in correlation with the mentioned introduction of copper into the ceria lattice and with changes in primary particle sizes (Table 1). Concerning the electronic state of copper, XAFS analyses (as also shown below) revealed that it appears in a fully oxidised Cu^{2+} chemical state with relatively small differences (except for the crystalline CuO detected in $5CuO/CeO_2$) between the samples concerning its electronic characteristics [25,27].

H_2-TPR profiles observed for the catalysts are displayed in Fig. 1. According to XPS results in a previous work and also in accordance with previous reports by other authors [6,32,33], the reduction peaks observed must be attributed to the reduction of copper in the samples although concomitant ceria reduction can also be produced [20,27,36,37], as also known to occur with other ceria-supported metals [38]. Indeed, quantitative estimation reveals overall H_2 consumption of 521, 1160, 542 and 1545 μmol per gram of catalyst for $1CuO/CeO_2$, $5CuO/CeO_2$, $Ce_{0.95}Cu_{0.05}O_2$ and $Ce_{0.8}Cu_{0.2}O_2$, respectively, which exceeds 157, 787, 297 and 1274 μmol g^{-1}, respectively required for the reduction of Cu only. Therefore, considering that the copper and cerium must be, as mentioned above, in fully oxidised states for the initial calcined samples, ceria reduction apparently also occurs. This appears particularly stronger for the samples prepared by impregnation (and especially for $1CuO/CeO_2$) while it decreases with the amount of copper in any of the two series. This indicates that ceria reduction during the process is mainly favoured by the presence of surface dispersed CuO species, i.e. by the number of CuO-ceria contacts. The lower overall relative reduction degrees comparatively achieved for the samples prepared by microemulsion-coprecipitation with lower copper content can also be related with the higher difficulty observed for the reduction of the part of copper introduced into the ceria fluorite structure (Fig. 2) [25,30].

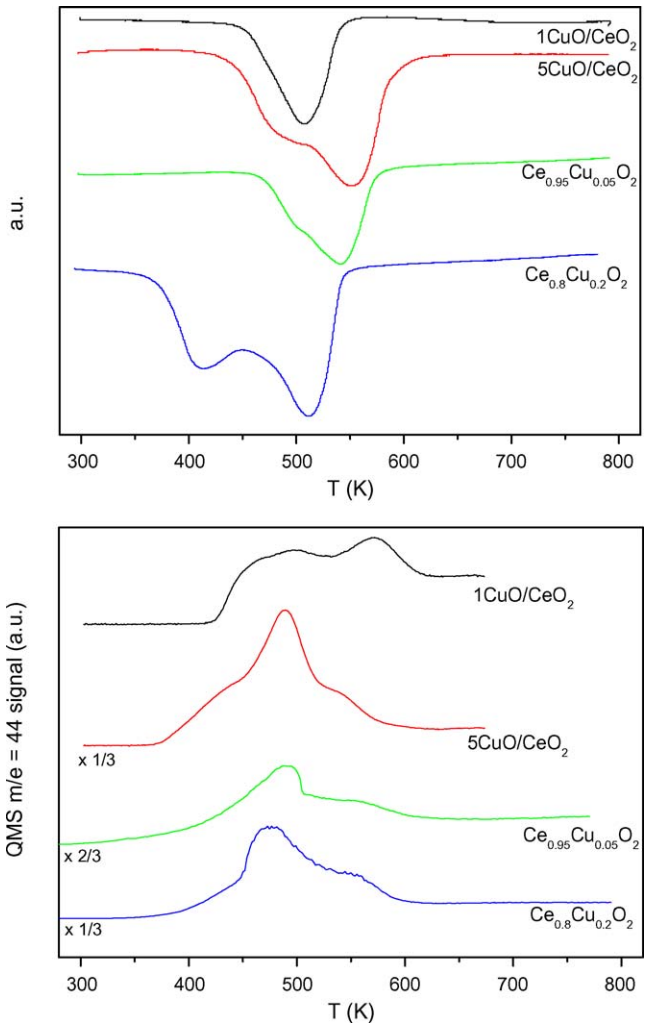

Fig. 1. H_2-TPR (TCD detector), top, and CO-TPR (QMS detector), bottom, profiles obtained for the indicated catalysts.

According to previous results in the literature [29–31], and as it has also been observed by us during TPR calibration experiments with pure CuO, the possible sequential reduction of copper ($Cu^{2+} \rightarrow Cu^{+} \rightarrow Cu^{0}$) is difficult to resolve in these experiments, so the different features observed in the samples must be related to structural/morphological differences in the copper oxide entities involved. In this respect, the TPR profiles observed (Fig. 1) clearly reveal the higher copper heterogeneity produced upon increasing the copper loading for any of the two preparation methods employed and in agreement with characterization results described above [27].

Thus, the presence of two well separated reduction peaks in $5CuO/CeO_2$ must be related to the presence of two different copper components in this sample (Table 1). In accordance with previous works [17,30–32], the component of copper dispersed on ceria (and therefore interacting with it) is responsible for the lowest temperature reduction peak (whose reduction onset appears at slightly lower temperature than for $1CuO/CeO_2$, suggesting the latter could have somewhat higher size for such dispersed CuO particles) while the peak at highest reduction temperature must be related to the reduction of the well formed CuO crystals present in this sample. In the case of $Ce_{0.8}Cu_{0.2}O_2$, the presence of two well separated reduction peaks certainly reflects also the heterogeneity of copper entities present in this sample, as noted above. The lowest temperature reduction peak present in this sample must be

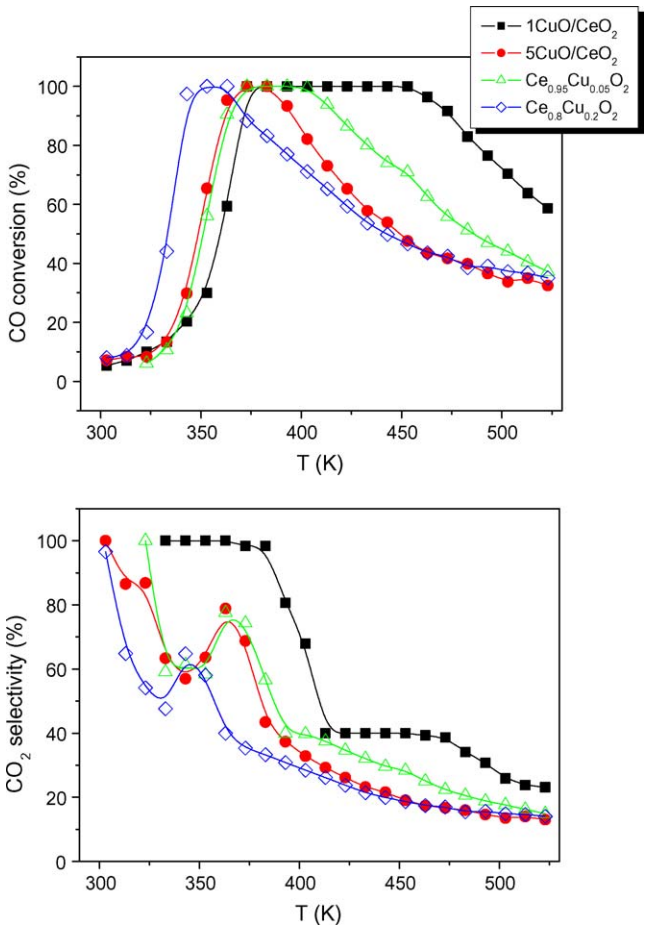

Fig. 2. Catalytic activity under 1% CO, 1.25% O_2 and 50% H_2 (Ar balance) obtained with the tubular catalytic reactor for the indicated catalysts. Top: CO conversion. Bottom: selectivity to CO_2.

due to the reduction of the surface segregated CuO clusters (more easy to be reduced than dispersed copper in $1CuO/CeO_2$, which is likely due to either size differences, smaller in $Ce_{0.8}Cu_{0.2}O_2$, or to different promoting effects by respectively CeO_2 and $Ce_{1-z}Cu_zO_2$ mixed oxide acting as a support in each case) while the peak at highest reduction temperature must be due to reduction of (at least a part) copper incorporated to the fluorite lattice. This latter component apparently predominates in $Ce_{0.95}Cu_{0.05}O_2$; differences in the respective reduction temperatures for this component between the two $Ce_{1-x}Cu_xO_2$ samples must be related to differences in the oxygen mobilities or promoting effects (on hydrogen activation, for instance) by previously reduced dispersed entities.

CO-TPR profiles, shown in Fig. 1, appear more complex likely as a consequence of involvement of diverse phenomena in addition to catalyst reduction; this can include CO or CO_2 chemisorption in the form of carbonates, stabilization of partially reduced states of copper (sequential instead of one step reduction) and possible occurrence of CO disproportionation reaction at high temperature that can be responsible for the uncomplete baseline recovery observed at high temperature [39,40]. Detailed individual characterization of these processes is in due course in our laboratory in order to achieve a complete assignment of the TPR features obtained when using CO as reductant. In any case, the results of Fig. 1 generally reveal a somewhat highest reducing power of CO with respect to H_2 for these samples, in agreement with previous work [5,12]. Such difference is also in agreement with operation of the systems by means of a redox mechanism in which CO and H_2 basically compete for oxygens at the active dispersed copper oxide entities or copper oxide-ceria interfaces [6,12]. In accordance with this hypothesis, it can be noted that comparative analysis of the reduction temperatures observed during these TPR experiments (Fig. 1) appears, at least qualitatively, in agreement with activity results (Fig. 2). To interpret these results, it must be noted, as mentioned in the experimental part, that basically CO and H_2 combustion are the only reactions taking place under the examined conditions. The overall evolution observed in the CO conversion profile displaying a maximum conversion at intermediate reaction temperature is (as inferred also from analysis of

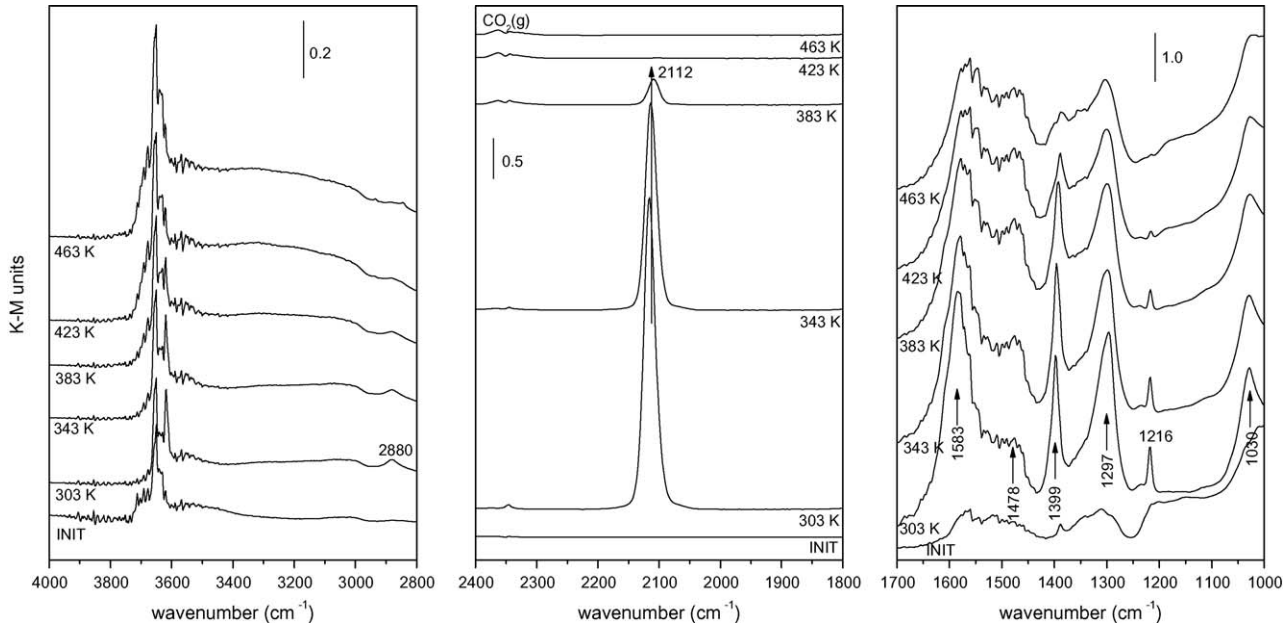

Fig. 3. DRIFTS spectra under $CO–H_2–O_2$ reactant mixture flow at the indicated temperatures for $1CuO/CeO_2$. The spectrum at the bottom corresponds to that recorded at 303 K after pretreatment under diluted O_2 at 773 K, prior to contact with the reactant mixture.

the CO_2 selectivity) a consequence of the competition between both combustion reactions, in accordance with results typically observed for this type of systems [3,4,6–13]. Basically, as discussed in more detail elsewhere [12], two regions can be generically differentiated in the activity profiles. The first one at low temperature (ca. <373 K, where the CO conversion increases) in which the competition between CO and H_2 for the active oxygen species is relatively weak [6,12]. A small promotion of H_2 oxidation by gaseous CO in this zone can explain the low temperature minimum observed in the CO_2 selectivity in some cases [12], Fig. 2. The second region corresponds to points above the maximum CO conversion (at relatively high reaction temperature), in which CO and H_2 strongly compete for the available active oxygen and which results in the strong high temperature decrease of CO_2 selectivity as a consequence of the significantly higher H_2 partial pressure within a redox Mars-van Krevelen kinetic scheme [6].

Appreciable differences are observed between the CO-PROX activity of the catalysts as a function of the copper loading and the preparation method employed (Fig. 2). It appears clearly that the oxidation activity of the catalysts (for both reductants) increases with the increasing copper loading in any of the series. Nevertheless, the balance between both oxidation reactions results in increases in CO_2 selectivities with the decreasing copper loading. These differences must be the consequence of differences in the specific characteristics of active components in each case. These likely include disperse CuO (considered as most active entities [30]) size and morphology, support nature (with a mixed oxide character in $Ce_{1-x}Cu_xO_2$ catalysts) and nature of the specific CuO-support contacts. In any case, it can be observed that onset of CO oxidation activity apparently takes place in any of the systems at lower temperature than corresponding reduction by individual CO, considering the CO-TPR profiles of Fig. 1. This seems in some contradiction with claimed Mars-van Krevelen character of the mechanism; however, relevant redox information can be missing at low temperature in the classical TPR runs, as recently demonstrated in a study by in situ CO-TPR-DRIFTS of CuO/$Ce_{1-x}Tb_xO_2$ catalysts [40]. It must also be noted in this sense that previous spectroscopic information (by EPR and XPS) indicated that some degree of copper reduction can take place even at sub-ambient temperature in this type of catalysts [18,20,27,29,36], and that the magnitude of possible mutual H_2-CO promoting effects is expected to be relatively low and could not explain such discrepancies [12].

In order to get hints on the reasons for the catalytic differences observed as well as achieving further details on the redox processes taking place, the systems were examined by *operando*-DRIFTS and XANES. Concerning DRIFTS experiments, the formation of bands of a similar nature for all catalysts was noted upon contact with the reactant mixture at reaction temperatures between 303 and 523 K. These basically appear in three distinct spectral zones, as illustrated in Fig. 3 for the $1CuO/CeO_2$ catalyst. The first zone displays bands corresponding mainly to hydroxyl species (isolated ones of various types giving sharp bands in the 3720–3600 cm^{-1} range and associated species giving a broad band extending from ca. 3800 to 3000 cm^{-1}) [41,42]. A second spectral zone below 1700 cm^{-1} exhibits bands due to carbonate or related species [42–45]. Most intense peaks in this zone are ascribed to bidentate carbonates at ca. 1583 and 1297; a combination band at ca. 2880 cm^{-1} (see the highest wavenumber zone at the left of Fig. 3), particularly apparent in lower temperature spectra, is also attributed to these species. Polydentate carbonates showing the symmetric and antisymmetric stretching of the terminal CO bonds at ca. 1478 and 1356 cm^{-1} are also detected. The band at 1216 cm^{-1}, along with that at 1399 cm^{-1} and a shoulder at ca. 1600 cm^{-1}, are attributed to hydrogen carbonate species [42,45]; this is confirmed by the presence of a sharp OH stretching vibration at ca. 3618 cm^{-1} also belonging to these species which must be formed upon interaction of CO with monodentate hydroxyls (giving rise to a band at ca. 3710 cm^{-1} in the spectrum of the original sample) [42,45]. The other spectral zone (at intermediate frequencies) shows the formation of CO_2(g), in accordance with CO oxidation activity, and a carbonyl species (a Cu^+-carbonyl giving

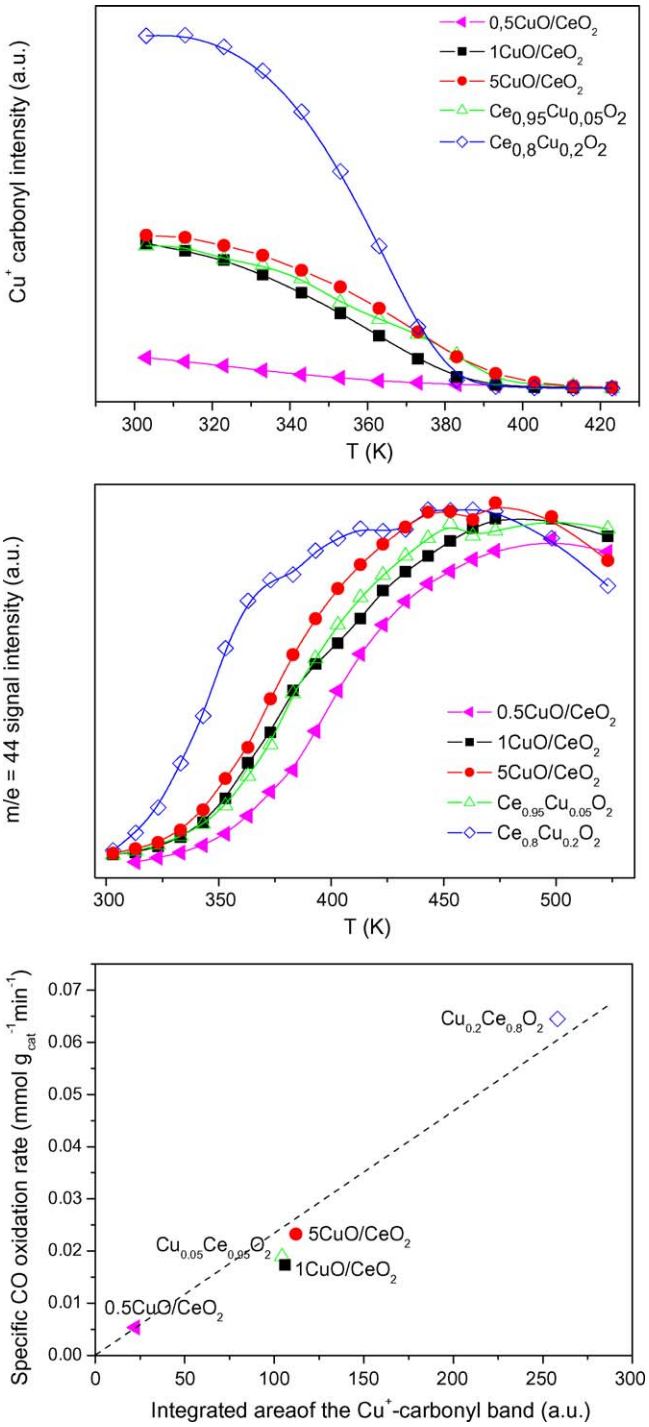

Fig. 4. Top: intensity of the Cu^+-carbonyl as a function of the reaction temperature under CO–H_2–O_2 mixture for the indicated catalysts. Middle: intensity of the QMS m/e = 44 signal, corresponding to CO_2, during the tests performed with the DRIFTS cell under CO–H_2–O_2 mixture. Bottom: correlation between the intensity of the Cu^+ carbonyl just prior to CO oxidation onset and the initial CO oxidation activity. The analysis is extended to a 0.5 Cu wt.% catalyst prepared by impregnation [27].

rise to a band at ca. 2120–2110 cm^{-1}; assignment according to previous reports, in which details can be found to justify this assignment) [18,36]. The presence of these Cu^{+}-CO species already upon initial contact at 303 K with the reactant mixture is consistent with the easy reduction of copper in the catalysts, considering that copper is fully oxidised in the initial calcined catalysts [27].

One of the main differences between the samples is related to the intensity of this Cu^{+}-carbonyl band. Furthermore, as displayed in Fig. 4, a correlation can be established between the intensity of such carbonyl and the CO oxidation activity of the samples. Considering that formation of such carbonyl species must be related to a support-promoted reduction process of the copper and taking also into account that the relatively low frequency of this band, with respect to those expected for this type of carbonyls [46], has been related to the interaction between these copper centres and the underlying ceria, this result clearly evidences that the active species for CO oxidation under CO-PROX conditions are related to surface dispersed partially reduced copper oxide species interacting with the support, i.e. at CuO-support interfacial positions. This is consistent with previous reports [18,20,27,36], which show that these copper species are easily reduced upon contact with CO at low temperature within a process in which the ceria support in contact with them can also become reduced [18,20,37,47]. Thus, differences between the CO oxidation activity under CO-PROX conditions for this type of catalysts must be related to the extent of support promotion of a partial CuO reduction at interfacial sites which is attained in each case.

Further support to this hypothesis is provided by *operando*-XANES. The analysis of the Cu-K-edge XANES spectra of $Ce_{0.8}Cu_{0.2}O_2$ and $5CuO/CeO_2$ indicates the presence of three different chemical species during the course of the runs. The first one corresponds to a Cu^{2+} chemical state displaying geometry similar to that found in CuO although displaying some particularities attributable to interactions with the support, as discussed in more detail elsewhere [25]. This component predominates at low reaction temperature, as illustrated by Fig. 5. In this sense, it must be noted that the level of copper reduction evidenced by DRIFTS at low temperature must correspond to a relatively low amount of the copper (note a maximal limit of ca. 10% as intrinsic error of the technique/analysis), exclusively related to interfacial sites in close interaction with the support which present the highest redox activity, in accordance with existence of a support promoting effect on the CuO reduction [20]. A component corresponding to zero-valent Cu^{0}, as identified from comparison with a Cu foil reference, predominates at the end of the runs (Fig. 5). An intermediate species is detected during spectra analysis and attributed to a Cu^{+} state on the basis of its 1s → 4p/3d transition energy and spectral shape. Joint analysis of the evolutions of the various copper species and the gases evolving during the CO-PROX tests allow to separate different relevant zones (Fig. 5). The first one (zone I) at lowest reaction temperature involves basically CO oxidation and has been discussed above on the basis of DRIFTS experiments. The second zone (II) displays a correlation between onset of H_2 oxidation and, at slightly lower temperature, onset of massive copper reduction to Cu^{+}. This correlation indicates the involvement of the latter species in H_2 oxidation, in agreement with the high reactivity shown by partially reduced copper oxide towards hydrogen [48]. Note that, as a difference with CO oxidation, H_2 oxidation takes place when the reduction is propagated to zones of the copper oxide nanoparticles not strictly in contact with the support. In this respect, H_2 oxidation can be most dependent on the specific properties (size, shape [49]) of the dispersed copper oxide nanoparticles, as pointed out previously [10]. In contrast, CO oxidation properties are most likely governed by the characteristics of the CuO-support contacts, i.e. the interfacial properties [28]. The third zone (III) is detected at higher temperature during H_2 oxidation in which the reaction rate changes in coincidence

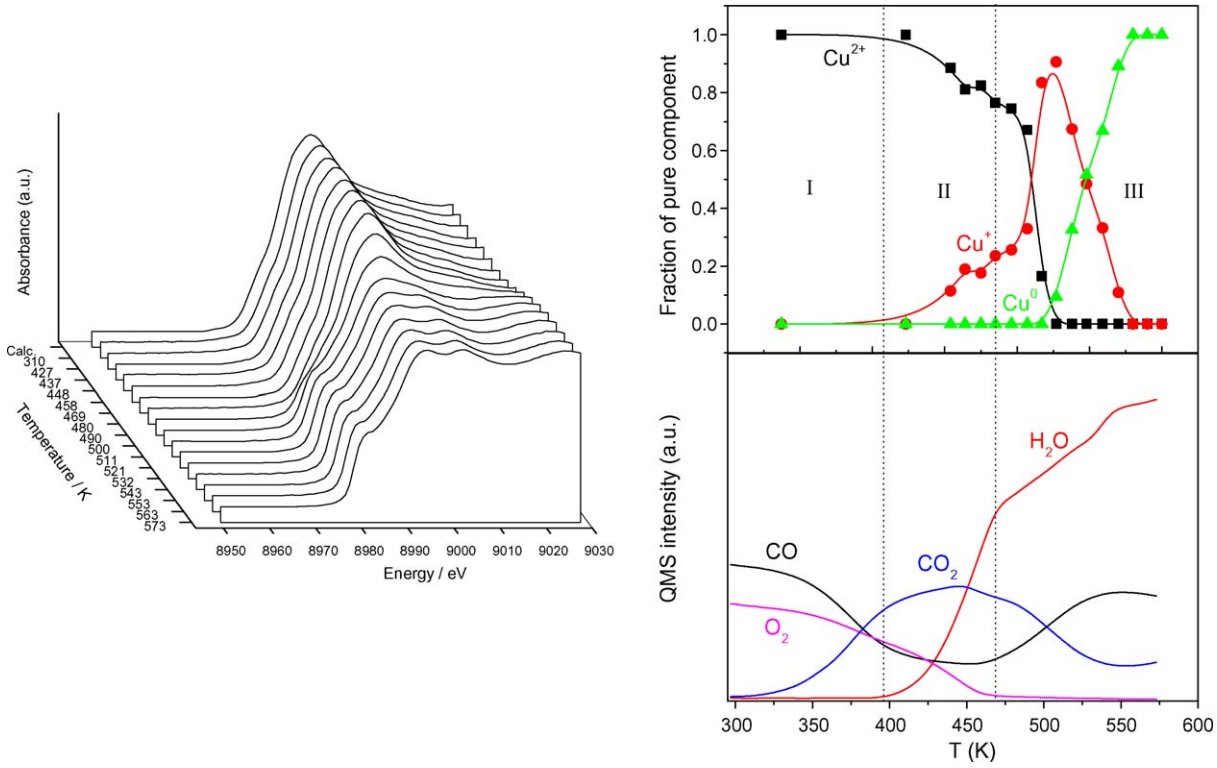

Fig. 5. Cu-K edge XANES spectra under $CO–H_2–O_2$ mixture over $Ce_{0.8}Cu_{0.2}O_2$ (left). Evolution of chemical species extracted from spectra analysis and of the various gases detected in the course of the *Operando* test with the XAFS cell (right).

with a sharp increase in the Cu^+ contribution. This can be related to the formation of less active Cu_2O and/or to sintering of the copper prior to generation of metallic copper [27,48]. This is detected at the highest reaction temperature and its formation fairly coincides with appearance of Ce^{3+} (not shown; see [28] for details). Certainly, the copper segregation produced by this reduction process can contribute to the small deactivation observed in these types of systems when maintained under the reactant mixture at relatively high temperature [7,12]. Validation of the correlations observed for $Ce_{0.8}Cu_{0.2}O_2$ is provided by observation of similar ones for $5CuO/CeO_2$ [28].

4. Conclusions

Redox-catalytic correlations in oxidised copper-ceria CO-PROX catalysts are shown to involve support promoting effects on the partial reduction of interfacial sites in dispersed CuO entities for CO oxidation while massive reduction of such entities apparently provides sites active for H_2 oxidation. Although qualitative correlations can be established on the basis of classical TPR analyses, important redox details are apparently missing in such tests. In contrast, *operando*-DRIFTS and XANES results allow getting relevant insights on the entities/species and/or phenomena involved during the two (CO and H_2) oxidation reactions taking place during CO-PROX tests over the catalysts. They demonstrate that CO oxidation takes place over interfacial positions of the partially reduced dispersed copper oxide entities since a correlation is established between such activity and the level of reduction achieved in such entities. The H_2 oxidation is shown to proceed immediately after onset of a massive copper reduction to Cu^+ indicating that active species for the process must be mainly related to partially reduced dispersed copper oxide nanoparticles. Copper segregation and formation of metallic copper occurs at $T >$ ca. 473 K and can contribute to the partial deactivation observed for this type of systems under the CO-PROX mixture. The apparent separation of the two types of sites that can be involved during the two (H_2 and CO) main oxidation processes which determine the CO-PROX performance of this type of systems opens the possibility to control their catalytic properties for this important application.

Acknowledgements

D.G. and A.H. thank the Ministerio de Educación y Ciencia (MEC) for the FPI and FPU PhD grants, respectively. P.B. thanks the 6th European Community Framework Marie Curie IIF program for a post-doctoral fellowship. The help provided by Dr. C. Belver and Dr. S.G. Fiddy at SRS station 7.1 (project # 44072) during recording of XANES spectra is greatly acknowledged. Thanks are due to the MEC (project CTQ2006-15600/BQU), and Comunidad de Madrid (project ENERCAM S-0505/ENE/000304) and CSIC-HAS bilateral agreement (2006HU0011) for financial support.

References

[1] J.R. Rostrup-Nielsen, J. Sehested, J.K. Norskov, Adv. Catal. 47 (2002) 65.
[2] Q. Fu, H. Saltsburg, M. Flytzani-Stephanopoulos, Science 301 (2003) 935.
[3] G. Avgouropoulos, T. Ioannides, Ch. Papadopoulou, J. Batista, S. Hocevar, H.K. Matralis, Catal. Today 75 (2002) 157.
[4] S.H. Oh, R.M. Sinkevitch, J. Catal. 142 (1993) 254.
[5] J.B. Wang, S. Lin, T. Huang, Appl. Catal. A 232 (2002) 107.
[6] G. Sedmak, S. Hocevar, J. Levec, J. Catal. 213 (2003) 135.
[7] D.H. Kim, J.E. Cha, Catal. Lett. 86 (2003) 107.
[8] Y. Liu, Q. Fu, M. Flytzani-Stephanopoulos, Catal. Today 93–95 (2004) 241.
[9] G. Marbán, A.B. Fuertes, Appl. Catal. B 57 (2005) 43.
[10] A. Martínez-Arias, A.B. Hungría, M. Fernández-García, J.C. Conesa, G. Munuera, J. Power Source 151 (2005) 32.
[11] F. Mariño, C. Descorme, D. Duprez, Appl. Catal. B 58 (2005) 175.
[12] A. Martínez-Arias, A.B. Hungría, G. Munuera, D. Gamarra, Appl. Catal. B 65 (2006) 207.
[13] J.-W. Park, J.-H. Jeong, W.-L. Yoon, H. Jung, H.-T. Lee, D.-K. Lee, Y.-K. Park, Y.-W. Rhee, Appl. Catal. A 274 (2004) 25.
[14] M. Jobbagy, F. Mariño, B. Schönbrod, G. Baronetti, M. Laborde, Chem. Mater. 18 (2006) 1945.
[15] E. Moretti, M. Lenarda, L. Storaro, A. Talon, T. Montanari, G. Busca, E. Rodríguez-Castellón, A. Jiménez-López, M. Turco, G. Bagnasco, R. Frattini, Appl. Catal. A 335 (2008) 46.
[16] A. Martínez-Arias, J. Soria, R. Cataluña, J.C. Conesa, V. Cortés Corberán, Stud. Surf. Sci. Catal. 116 (1998) 591.
[17] W. Liu, A.F. Sarofim, M. Flytzani-Stephanopoulos, Chem. Eng. Sci. 49 (1995) 4871.
[18] A. Martínez-Arias, M. Fernández-García, O. Gálvez, J.M. Coronado, J.A. Anderson, J.C. Conesa, J. Soria, G. Munuera, J. Catal. 195 (2000) 207.
[19] B. Skårman, D. Grandjean, R.E. Benfield, A. Hinz, A. Andersson, L.R. Wallenberg, J. Catal. 211 (2002) 119.
[20] A. Martínez-Arias, A.B. Hungría, M. Fernández-García, J.C. Conesa, G. Munuera, J. Phys. Chem. B 108 (2004) 17983.
[21] A.N. Ilichev, A.A. Firsova, V.N. Korchak, Kinet. Catal. 47 (2006) 585.
[22] G. Avgouropoulos, T. Ioannides, H. Matralis, Appl. Catal. B 56 (2005) 87.
[23] A. Tschöpe, M.L. Trudeau, J.Y. Ying, J. Phys. Chem. B 103 (1999) 8858.
[24] P. Bera, K.R. Priolkar, P.R. Sarode, M.S. Hegde, S. Emura, R. Kumashiro, N.P. Lalla, Chem. Mater. 14 (2002) 3591.
[25] X.Q. Wang, J.A. Rodriguez, J.C. Hanson, D. Gamarra, A. Martínez-Arias, M. Fernández-García, J. Phys. Chem. B 109 (2005) 19595.
[26] W. Shan, W. Shen, C. Li, Chem. Mater. 15 (2003) 4761.
[27] D. Gamarra, G. Munuera, A.B. Hungría, M. Fernández-García, J.C. Conesa, P.A. Midgley, X.Q. Wang, J.C. Hanson, J.A. Rodríguez, A. Martínez-Arias, J. Phys. Chem. C 111 (2007) 11026.
[28] D. Gamarra, C. Belver, M. Fernández-García, A. Martínez-Arias, J. Am. Chem. Soc. 129 (2007) 12064.
[29] D. Gamarra, A. Hornés, Zs. Koppány, Z. Schay, G. Munuera, J. Soria, A. Martínez-Arias, J. Power Source 169 (2007) 110.
[30] M.-F. Luo, Y.-P. Song, J.Q. Lu, X.-Y. Wang, Z.-Y. Pu, J. Phys. Chem. C 111 (2007) 12686.
[31] M.-F. Luo, J.-M. Ma, J.-Q. Lu, Y.-P. Song, Y.-J. Wang, J. Catal. 246 (2007) 52.
[32] A. Pintar, J. Batista, S. Hocevar, J. Coll. Interf. Sci. 285 (2005) 218.
[33] M. Manzoli, R. Di Monte, F. Bocuzzi, S. Coluccia, J. Kaspar, Appl. Catal. B 61 (2005) 192.
[34] A. Martínez-Arias, M. Fernández-García, V. Ballesteros, L.N. Salamanca, J.C. Conesa, C. Otero, J. Soria, Langmuir 15 (1999) 4796.
[35] M. Fernández-García, Catal. Rev. Sci. Eng. 44 (2002) 59.
[36] A. Martínez-Arias, M. Fernández-García, J. Soria, J.C. Conesa, J. Catal. 182 (1999) 367.
[37] A. Martínez-Arias, D. Gamarra, M. Fernández-García, X.Q. Wang, J.C. Hanson, J.A. Rodríguez, J. Catal. 240 (2006) 1.
[38] J.P. Holgado, G. Munuera, Stud. Surf. Sci. Catal. 96 (1995) 109.
[39] J. Papavasiliou, G. Avgouropoulos, T. Ioannides, Catal. Commun. 5 (2004) 231.
[40] P. Bera, A. Hornés, D. Gamarra, A.B. Hungría, M. Fernández-García, G. Munuera, A. Martínez-Arias, in: Proceedings of 14th International Congress on Catalysis, Seoul, Korea, 2008.
[41] A. Badri, C. Binet, J.-C. Lavalley, J. Chem. Soc. Faraday Trans. 92 (1996) 4669.
[42] C. Binet, M. Daturi, J.-C. Lavalley, Catal. Today 50 (1999) 207.
[43] C. Li, Y. Sakata, T. Arai, K. Domen, K.-I. Maruya, T. Onishi, T.J. Chem, Soc. Faraday Trans. 1 (85) (1989) 929.
[44] C. Li, Y. Sakata, T. Arai, K. Domen, K.-I. Maruya, T. Onishi, T.J. Chem, Soc. Faraday Trans. 1 (85) (1989) 1451.
[45] O. Pozdnyakova, D. Teschner, A. Wootsch, J. Kröhnert, B. Steinhauer, H. Sauer, L. Toth, F.C. Jentoft, A. Knop-Gericke, Z. Paál, R. Schlögl, J. Catal. 237 (2006) 1.
[46] D. Scarano, S. Bordiga, C. Lamberti, G. Spoto, G. Ricchiardi, A. Zecchina, C. Otero Areán, Surf. Sci. 411 (1998) 272.
[47] A. Martínez-Arias, M. Fernández-García, A.B. Hungría, A. Iglesias-Juez, O. Gálvez, J.A. Anderson, J.C. Conesa, J. Soria, G. Munuera, J. Catal. 214 (2003) 261.
[48] J.Y. Kim, J.A. Rodriguez, J.C. Hanson, A.I. Frenkel, P.L. Lee, J. Am. Chem. Soc. 125 (2003) 10684.
[49] M. Fernández-García, A. Martínez-Arias, J.C. Hanson, J.A. Rodríguez, Chem. Rev. 104 (2004) 4063.